Predicting Depth of Cut of Water-jet in Soft Tissue Simulants based on Finite Element Analysis with the Application to Fracture-directed Water-jet Steerable Needles

Mahdieh Babaiasl[1], Fan Yang[2], Yao Chen[3], Jow-Lian Ding[4], and John P. Swensen[5]

***Abstract*— Water-jet technology has been used recently in medical applications including surgery, soft tissue resection, bone cutting, and wound debridement. The ability to measure the depth of cut of water-jet is important in these applications to selectively cut the desired tissue, and avoid damage to deeper layers. For fracture-directed water-jet steerable needles, one should be able to predict the depth of cut of water-jet in order to model the motion of the steerable needle. In this paper, the effect of tissue stiffness, water-jet flow rate, and nozzle diameter on depth of cut is studied experimentally and verified by finite element modeling. It is found that the depth of cut of water-jet has a direct relationship with flow rate, and an inverse relationship with elastic modulus of the tissue, and diameter of the needle. The proposed finite element model can predict the depth of cut with acceptable accuracy.**

I. INTRODUCTION

Water-jet has already been used in several industrial applications such as mining, cutting materials, drilling, and cleaning. Recently, this technology has been used in medical applications [1] such as in surgery for dissection of organs [2], [3], dentistry, bone cutting [4], and wound debridement [5]. The advantages of using water-jet as a cutting tool are its precision, speed, and it can be as effective as a laser cutter without the thermal damage to surrounding tissues. Water-jet also washes away the blood during surgery, and decreases bleeding [6]. These advantages made water-jet an appealing method for medical applications.

Measuring depth of cut of water-jet is important from medical applications point of view. For example, in surgical applications using water-jet, selective cutting is a must. In other words, water-jet should cut the desired layer and should not go further [7]. For instance, in order for the optimal performance of the Versajet water-jet surgical tool in treating the different depth face and neck burns, the depth of debridement should be controlled [8].

[1]Mahdieh Babaiasl is a graduate research assistant with the School of Mechanical and Materials Engineering, Washington State University, Pullman, Washington, USA. mahdieh.babaiasl@wsu.edu

[2]Fan Yang is a graduate research assistant with the School of Mechanical and Materials Engineering, Washington State University, Pullman, Washington, USA. fan.yang6@wsu.edu

[3]Yao Chen is a graduate research assistant with the School of Mechanical and Materials Engineering, Washington State University, Pullman, Washington, USA. yao.chen@wsu.edu

[4] Jow-Lian Ding is a professor with the School of Mechanical and Materials Engineering, Washington State University, Pullman, Washington, USA. jowlian_ding@wsu.edu

[5]John P. Swensen is an assistant professor with the School of Mechanical and Materials Engineering, Washington State University, Pullman, Washington, USA. john.swensen@wsu.edu

978-1-5386-7825-1/19/$31.00 ©2019 IEEE

In this paper, the effect of tissue stiffness, needle diameter, and flow rate of water-jet on depth of cut of water-jet needle has been studied experimentally. A finite element model is also developed to predict the depth of cut. Predicting depth of cut is the first step to model the motion of fracture-directed water-jet steerable needles [9]. In water-jet steerable needles, the needle has a fixed angle nozzle that can cut a small channel at an angle in the tissue while running the pump at specific flow rate. The pump will be turned off, and the needle will be inserted equally to the depth of cut channel. Because of the difference in bending stiffnesses of the needle and the tissue, as well as the elastic equilibrium between the needle and the tissue, the needle will bend. This process continues until the needle can be steered in the tissue. Modeling the motion of the steerable needle requires that we predict the depth of cut channel and thus how far the needle should be pushed into the tissue. Fig. 1 shows an example of before, and after of an experiment to measure the cut depth.

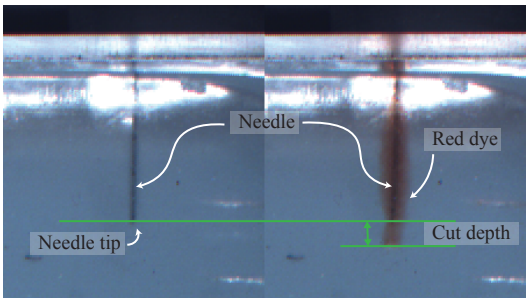

Fig. 1. Definition of depth of cut for a water-jet needle [9].

II. MATERIALS AND METHODS

A. Soft Tissue Substitute Preparation and Compressive Tests

Due to the difficulties associated with using, storing, and imaging of real biological tissues, different researchers have utilized substitute materials for experiments that can provide an average approximation of the soft tissue [10], [11], [12], [13], [14]. Gelatin, rubbers, leather, silicone elastomers, PVA, and lard are among common materials for tissue mimicking simulants [10]. The mechanical properties of water-based tissue simulants such as gelatin can be changed with respect to time, temperature, and humidity change.

In this paper we have used Poly (styrene-b-ethylene-co-butylene-b-styrene) triblock copolymer (SEBS), Kraton Polymers LLC (G1650, and G1652, Houston, TX, USA)

as the main material for soft tissue simulants. Having a non-aqueous solvent (light mineral oil) makes SEBS a more environmentally stable substitute for water-based hydrogels with increased operational temperature ranges, and shelf life. One major advantage of soft tissue simulants made out of SEBS is that they are optically clear, which is desirable from imaging point of view. The stiffness of SEBS can be easily changed by altering the polymer content to make tissues with low Young's moduli and high fracture toughnesses similar to biological tissues. SEBS has also low friction (due to oil solvent) than other materials with low Young's moduli such as silicone rubbers.

To make the tissue simulants, SEBS material and mineral oil are weighed out to produce mixtures with 10, 15, and 20 vol% SEBS. To calculate the necessary weight, the densities of SEBS, and mineral oil are considered to be $\rho_{SEBS} = 0.91\frac{g}{cm^3}$, and $\rho_{oil} = 0.85\frac{g}{cm^3}$, respectively. The mixture is then put in the oven at 150^oC for about 2 to 8 hours based on the percentage of SEBS, and it was mixed from time to time to get a homogeneous solution without any undissolved powder. After this time, the solution is degassed to eliminate any air bubbles trapped in the solution. The solution is then poured into rectangular molds of the dimensions $100 \times 100 \times 50$ mm sprayed with mold release, and then let cool down to room temperature and solidify before releasing from the molds.

The static compression tests were conducted with an Instron 600DX machine. All the samples were molded to have a same diameter of 30 mm and thickness of 10 mm. In the tests, the samples were compressed between two parallel metal plates with a same strain rate of $\frac{10^{-3}}{s}$. The force was measured with a 25 lb (about 111 N) S-beam load cell, and the displacement was measured with the build-in function of the machine. The data acquisition rate was set to be 10 Hz for both the load and displacement. The applied force and relative displacement of the metal plates were converted to engineering stress (sigma symbol) and engineering strain (epsilon symbol) as follows: $\sigma = \frac{4F_{CL}}{\pi d_s^2}$, and $\varepsilon = \frac{\Delta L}{h}$ where F_{CL}, d_s, ΔL, and h are the compressive load measured with the load cell, the original diameter of the sample, the change in thickness due to compression, and the initial thickness of the sample, respectively.

B. Experimental Setup and Measurement of Depth of Cut of Water-jet in Soft Tissue Simulants

The experimental setup used for all experiments is depicted in Fig. 2. A linear actuator is used to drive the needle with the velocity of insertion of $1\frac{mm}{s}$ approximately $1cm$ into the soft tissue simulant. A high pressure pump (PR-class Dual Piston, PR100PFT3D, Scientific Systems Inc., State College, PA, USA) provides a constant volumetric flow rate (up to $100\frac{mL}{min}$) and when run, water-jet needle will cut a channel in front of it in the tissue. After about 30 seconds, the camera takes a photo and the photo will be processed in image processing software to measure the depth of cut of water-jet. 3D-printed custom-designed box along with suction canister, and a vacuum pump are used to collect the water sprayed back during experiments.

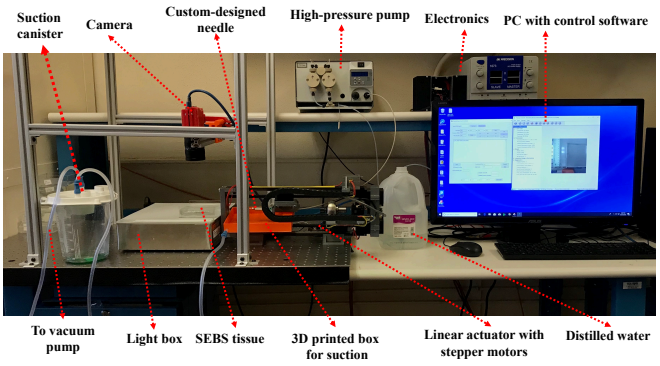

Fig. 2. Experimental setup of the water-jet needle system to measure the depth of cut of water-jet.

For the water-jet needle, first a piece of Nitinol tube is cut to a length of 52.8 mm. Next, the Nitinol tube is soldered inside the copper tube of 45 mm length with inner diameter of $ID = 0.94$ mm, and outer diameter $OD = 1.59$ mm. Finally, the copper tubing is attached to the ferruled reducer and then to the water pump via PEEK tubing ($ID = 1.58$ mm, and $OD = 3.2$ mm). Two needles were manufactured with two different diameters to study the effect of diameter of the needle on depth of cut. The first needle has Nitinol tube with $ID = 0.32$ mm, and $OD = 0.58$ mm, and the Nitinol tube of the second needle has $ID = 0.24$ mm, and $OD = 0.33$ mm. Fig. 3 shows the first designed needle (the second needle is the same only with a different diameter Nitinol tube).

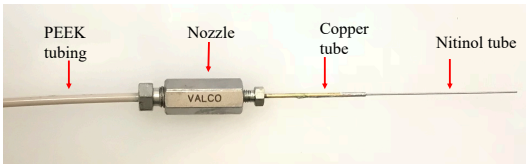

Fig. 3. Custom-designed water-jet needle with a copper tubing ($ID = 0.94$ mm, and $OD = 1.59$ mm) soldered to a superelastic material Nitinol (first needle: $ID = 0.32$ mm, and $OD = 0.58$ mm, and second needle: $ID = 0.24$ mm, and $OD = 0.33$ mm). The copper tubing is attached to a ferruled reducer, and then standard PEEK tubing.

To measure the depth of cut of water-jet in SEBS tissue, the pump is turned on with the specific flow rate and the water-jet needle is inserted into soft tissue about 1 cm using the linear actuator and with velocity of insertion of $1\frac{mm}{s}$. This will ensure that the excess water will be sprayed back and will not be trapped in the channel to cause ballooning in the tissue. When the needle is inserted 1 cm into the tissue, the pump will be turned off and turned on again to ensure maximum depth of cut. After 30 seconds, and using the overhead high-resolution camera and the control software, a photo is taken and saved for further processing. For better visibility, edible food dye was added to the water. To study the effects of tissue stiffness, needle diameter, and flow rate on cut depth, 3 different tissue stiffnesses (10 %,

15 %, and 20 % G1650 SEBS), 2 different needle diameters (first needle: $ID = 0.32$ mm, $OD = 0.58$ mm, and second needle: $ID = 0.24$ mm, $OD = 0.33$ mm), and different flow rates up to $100\frac{mL}{min}$ are tested. To make sure that the data are statistically significant, 5 experiments are done for each flow rate and the average of them is taken as the cut depth. The photos are processed using a customized Matlab program that measures the depth of cut in front of the needle from the pixels of the photo based on the calibrated measurement provided by the ruler on the light-box.

C. Prediction of Depth of Cut of Water-jet using Finite Element Modeling

In order to have a predictive model for depth of cut of water-jet in tissue simulants, a finite element model was developed. Since a soft solid is interacting the liquid water, the case can be assumed to be a fluid-soft solid interaction. Therefore, a system to analyze the fluid flow in the needle and a system to analyze the structural deformation of the soft solid should be deployed. Since the data from both systems are inter-dependent, both systems are coupled together to form an FSI (fluid-solid interaction) solver.

The flow regimes of water inside the needle can be either laminar or turbulent. The critical flow rate, which is the highest flow rate ($\frac{mL}{min}$) to achieve laminar flow in the specific section of the tube can be calculated by the Equation 1.

$$Q_{critical} = \frac{Re_{critical}\pi d_{tube} u}{4\rho \times 1000 \times 1000 \times 60} \tag{1}$$

In which, $Re_{critical}$ is the critical Reynolds number where flow transitions from laminar to turbulent and is considered to be $Re_{critical} = 2300$, ρ, u, and d_{tube} are the density $\frac{kg}{m^3}$ (for water: *rho* = 997), dynamic viscosity $\frac{kg}{ms}$ ($u = 0.891 \times 10^{-3}$), and diameter of the tube in meters, respectively. The above equation gives the critical flow rate in $\frac{mL}{min}$. The critical flow rates for 0.32 mm, and 0.24 mm needles are 30.99, and 23.24 $\frac{mL}{min}$, respectively. Therefore, two different models for laminar and turbulent cases have been applied to determine the pressure parameters in finite element modeling.

In order to determine the depth of cut of water-jet in the finite element modeling, the solution algorithm depicted in Fig. 4 is used for laminar and turbulent flow regimes. Since the pump provides volumetric flow rate, Q_{pump} ($\frac{m^3}{s}$), and the inlet and outlet of the software are mass flow rate, the following equation is used to calculate the mass flow rate, $\dot{m}$ ($\frac{kg}{s}$):

$$\dot{m} = \rho Q_{pump} \tag{2}$$

In this equation, ρ ($\frac{kg}{m^3}$) is the density of the liquid (in this case, water).

CFX solver, and Transient Structural Solver in ANSYS will cater for the fluid flow section, and Structural domain of the above algorithm, respectively. Both solvers will share the geometry and the solution data from CFX to the Transient Structural. The tissue is modeled as a cube with the sides of

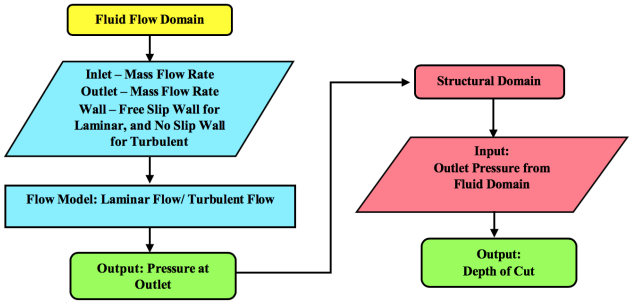

Fig. 4. Finite element solution algorithm for laminar and turbulent flow regimes

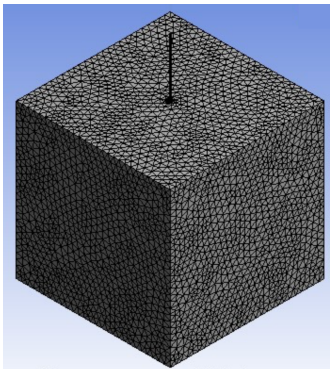

Fig. 5. Model of tissue and the needle in ANSYS. The tissue is modeled as a cube with 40 mm sides, and the needle is modeled to the shape and diameter of each Nitinol tube.

length 40 mm. Fig. 5 depicts the model of tissue, and the needle.

In the CFX solver, the first layer thickness is $\frac{r}{38}$ for the mesh used in the laminar case. The first layer thickness is added as inflation, and the inner layers are meshed using Patch Conforming Tetra Mesh. For the boundary conditions, the water is set as the working material. The wall is considered as the wall of the needle and is assigned a free slip wall. The inlet, and outlet are assumed to be mass flow rate since the input and output flow rates are the same (the pump provides a constant flow rate). The Turbulent flow simulation is the same as laminar flow except Shear Stress Transport model is used, and for the boundary condition, the wall is considered as the wall of the needle and is assigned a no slip wall.

For the transient structural analysis, the pressure from the fluid flow analysis is imported into the structural solver. The needle penetrating into the soft tissue is meshed using a hex dominant mesh and the soft tissue is meshed using patch forming method. The quality obtained for hex dominant mesh is 0.85. In this mesh, 8792 nodes, and 5947 elements are used. The mesh used for the tissue simulant has a concentrated face mesh of size 1×10^{-3} near the pressure loaded area to capture the deformation of the soft tissue. An average element quality of 0.82 was achieved which is well within the permissible limits $(0.8 - 1)$ for the solution convergence. 62660 nodes, and 19451 elements are used.

Fig. 6 shows the soft tissue simulant with Patch Conforming Tetra mesh and the needle with Hex Dominant mesh.

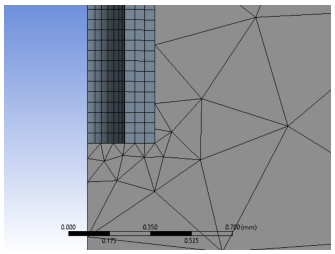

Fig. 6. Meshes used for needle penetration into the soft tissue simulant. The soft tissue, and the needle are meshed with Patch Conforming Tetra mesh, and Hex Dominant mesh, respectively.

The soft tissue simulant is assumed to be an isotropic material with the properties of table I. The strain is considered to be small. The specimen is given the boundary conditions of a fixed support on all 4 sides and bottom, and the pressure is automatically updated in the outlet region.

III. Results

In this section, results of the tests to measure the mechanical properties of SEBS, depth of cut of water-jet in soft tissue, and prediction of depth of cut with finite element modeling are provided.

A. Mechanical properties of SEBS based on Compressive tests

Fig. 7 shows the average Engineering Stress vs. strain response of G1650 SEBS tissue mimicking simulants from 3 experiments for each tissue. The Young's moduli of these tissues were determined from the slope of the linear section of the curves.

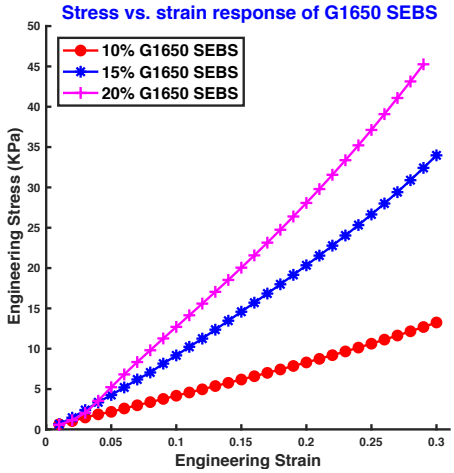

Fig. 7. Average Stress-strain curve of G1650 SEBS from 3 experiments for each tissue. The test strain rate is $\frac{10^{-3}}{s}$.

The mechanical properties of the SEBS tissue mimicking phantoms are summarized in table I. The Young's moduli of SEBS G1652 can be found from Equation 3, which we have derived from the log-log plot of the Young's modulus vs. polymer fraction figure presented in [10]. The measured stiffnesses are relevant to the stiffnesses of real biological tissues [15].

TABLE I
Mechanical properties of SEBS tissue-mimicking phantoms

Tissue phantom	density ($\frac{g}{cm^3}$)	Young's Modulus (kPa)	Poisson's ratio
10% G1650 SEBS	0.856	42.5	0.49
15% G1650 SEBS	0.859	112.9	0.49
20% G1650 SEBS	0.862	159.8	0.49
15% G1652 SEBS	0.859	68	0.49
20% G1652 SEBS	0.862	128	0.49

$$Young's\ modulus = c(Polymer\ fraction)^m \tag{3}$$

Where $c = 4.6018 \times 10^6$ and $m = 2.2234$.

B. Depth of Cut of Water-jet in Soft Tissue Stimulants is a Function of Needle Diameter, Tissue Stiffness, and Velocity of Water-jet

Fig. 8 shows the average measurements of depth of cut as a function of fluid velocity with different percentages of SEBS tissues, and needles with inner diameters of 0.24 mm, and 0.32 mm. Fig. 9, and Fig. 10 show the depth of cut of water-jet as a function of needle diameter, and tissue stiffness, respectively.

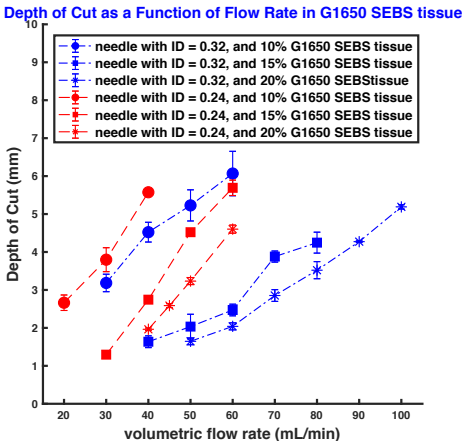

Fig. 8. Depth of cut of water-jet as a function of flow rate in G1650 SEBS tissue. Two different needles with different diameters, and 3 different tissue stiffnesses are used. The errorbars show the standard deviation of data from 5 experiments.

The following results can be derived from these experimental results:

- Depth of cut is almost a linear function of flow rate (Q_{pump}) when the width of the water-jet nozzle is sufficiently small.
- The depth of cut is a function of flow rate (Q_{pump}), modulus of elasticity (E_t) of the tissue, and needle diameter (d_n). It has a direct relationship with flow rate, and inverse relationship with tissue stiffness and needle diameter:

$DOC \sim Q_{pump}$
$DOC \sim \frac{1}{d_n.E_t}$

- There is a minimum flow rate that the fracture in the tissue actually begins, and this flow rate is dependent on the stiffness of the tissue. As the tissue becomes stiffer, larger flow rate is required to cause fracture in the tissue.
- For smaller diameter needle, the minimum flow rate needed to cut is lower. This is likely due to the higher contact stress which leads to the earlier fracture of the tissue. The higher residual jet velocity associated with smaller needle diameter after the initial penetration also leads to larger depth of cut.
- For higher flow rates, water cuts more of the surrounding tissue, which is undesirable. For fracture-directed steerable needles [16], larger depth of cut is not necessary and it is important that a small amount is cut and then the needle follows the path.
- Observation that the depth of cut of a smaller diameter needle is larger explains the reason of tissue fracture by water-jet. According to the equation 4, as the diameter of the needle decreases the velocity of water-jet increases and thus the kinetic energy of water-jet increases. The increased kinetic energy is the reason that the depth of cut of water-jet needle with smaller diameter is larger than that of with bigger diameter. In this equation, Q_{pump}, $d_{jet} = d_n$, and v_{ave} are volumetric flow rate, water-jet diameter, and velocity of water-jet, respectively.

$$v_{ave} = \frac{Q_{pump}}{A_{jet}} = \frac{4Q_{pump}}{\pi d_{jet}^2} \tag{4}$$

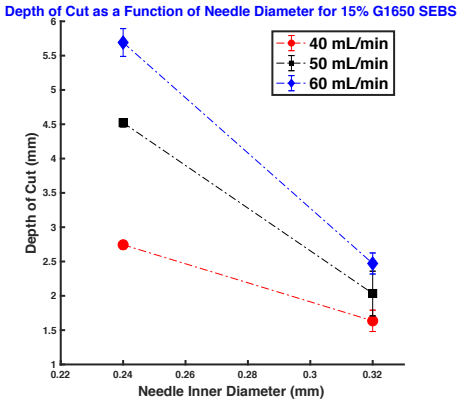

Fig. 9. Depth of cut of water-jet as a function of needle diameter shown as an example for 15% G1650 SEBS. The errorbars show the standard deviation of data from 5 experiments. The tissue stiffness, and flow rate are held constant here.

C. Finite Element Model of Soft Tissue and Water-jet Needle Can Predict the Depth of Cut with Acceptable Accuracy

The solution is solved for a time-step size of 30s with a minimum step size of 0.5s. The obtained deformation is visualized using the total deformation tool to evaluate the depth of cut as required. Fig. 11 is an example of the output

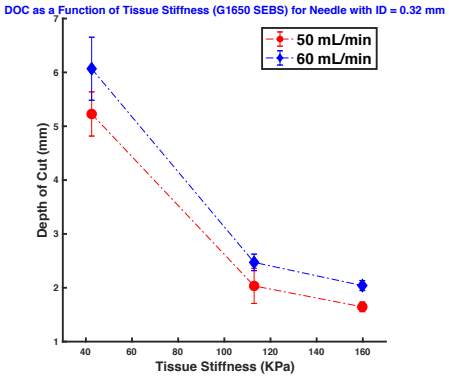

Fig. 10. Depth of cut of water-jet as a function of tissue stiffness shown as an example for 0.32 mm needle. The errorbars show the standard deviation of data from 5 experiments. The needle diameter, and flow rate are held constant here.

that shows that the deformation is interpreted as 3.5mm from the outlet of the needle.

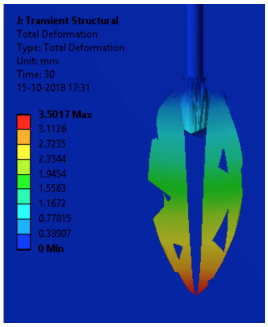

Fig. 11. Example output of the finite element modeling for depth of cut of water-jet. In this example, maximum depth of cut is interpreted from the outlet of the needle.

Fig. 12, Fig. 13, and Fig. 14 represent the experimental depth of cut and predicted depth of cut from finite element modeling in different G1650 SEBS tissues with 0.32 mm, and 0.24 mm water-jet needle, and G1652 SEBS tissues with 0.32 mm needle, respectively. There is an acceptable agreement between the experimental results and the predicted results by finite element modeling.

IV. Discussion

In this paper, first an experimental analysis is conducted to study the effect of flow rate, tissue stiffness, and needle diameter on the depth of cut of water-jet needle. A finite element model is proposed to predict the depth of cut of water-jet needle in soft tissue.

This research is conducted as a part of the research on fracture-directed water-jet steerable needles, in which a water-jet needle with a fixed-angle nozzle is inserted in the tissue, and then the pump is turned on and the water-jet cuts a small channel at nozzle angle in front of the needle. The pump is turned off, and the needle follows the cut channel. Because of the elastic equilibrium between the needle and the tissue, and difference between the bending stiffnesses of the needle, and the tissue, the needle will bend. The pump

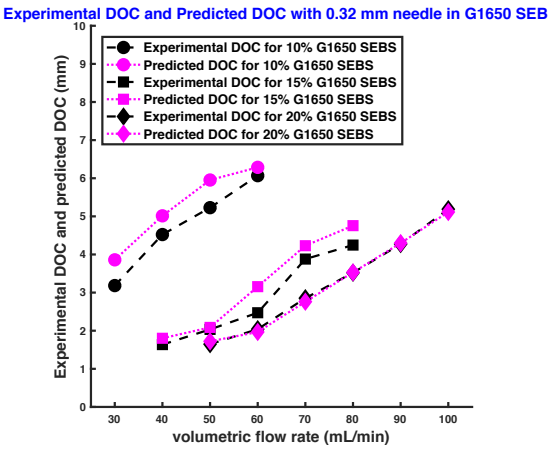

Fig. 12. Experimental depth of cut and predicted depth of cut with 0.32 mm needle in G1650 SEBS.

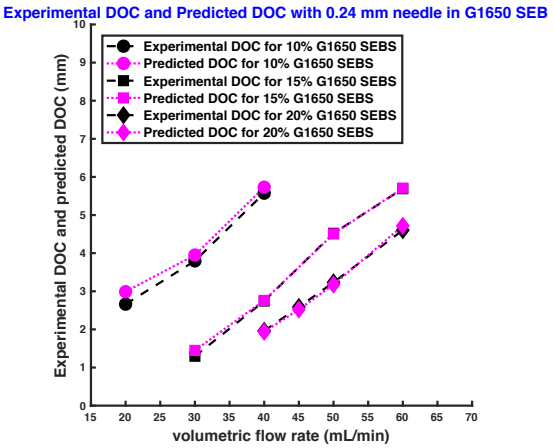

Fig. 13. Experimental depth of cut and predicted depth of cut with 0.24 mm needle in G1650 SEBS.

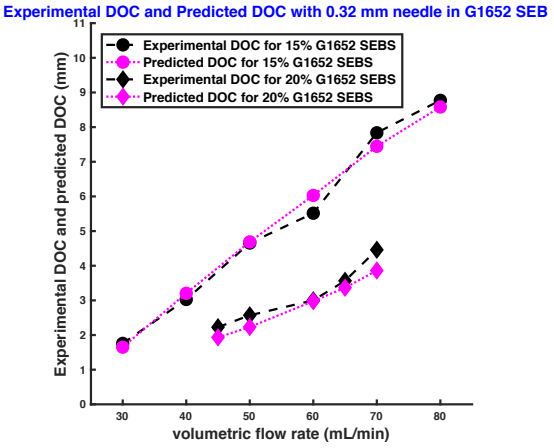

Fig. 14. Experimental depth of cut and predicted depth of cut with 0.32 mm needle in G1652 SEBS.

will be turned on again and another channel will be cut at an angle. The pump will be turned off and the needle follows the cut channel. This process continues and causes the needle to steer in the tissue. Fig. 15 shows a schematic of this method. In order to model the motion of the needle, predicting the depth of cut in front of the needle is necessary.

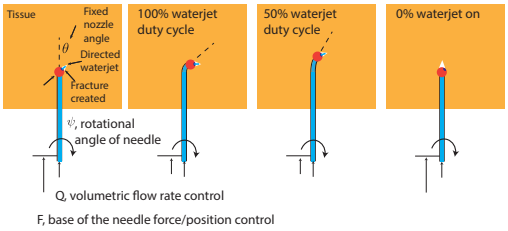

Fig. 15. Schematic of fracture-directed water-jet steerable needles. In this method, the needle follows a small channel cut by water-jet in tissue. Due to the difference between the bending stiffnesses of needle and tissue, and the elastic equilibrium between needle, and tissue, the needle bends and can be steered by duty cycling the water-jet. The first step in order to model the motion of the water-jet needle is to predict the length of the channel cut in front of the water-jet that will be the input to the motion model.

In this paper, only the effect of tissue elastic modulus (E), flow rate (Q), and the needle diameter (D) on depth of cut is investigated. Another important property that plays a role here is fracture toughness of the tissue. In order to have an accurate model, fracture toughness should also be considered. Research is underway to study the effect of this parameter on the depth of cut. Furthermore, we only considered the elastic moduli of the tissues measured at low strain rate. However, water-jet cutting involves high strain rate response of the tissue. Incorporating the high strain rate properties of the soft tissue in the model is left for future research.

V. CONCLUSIONS AND FUTURE WORK

In this paper the effect of tissue stiffness, needle diameter, and flow rate on depth of cut of water-jet needle was investigated experimentally, and a finite-element based model was proposed for prediction. Experimental results showed that depth of cut has a direct relationship with flow rate, and an inverse relationship with elastic modulus of the tissue and needle diameter.

This study only considered the effect of elastic modulus of the tissue, diameter of the needle, and flow rate of water-jet on the depth of cut. It also did not consider the high strain response of the tissue, which is the case for water jet cutting soft tissue. Future research involves also taking into account the effect of fracture toughness of the tissue on depth of cut, and high strain rate response of the soft tissue. Predictive mechanics-based model for depth of cut as a function of tissue and needle properties based on the experimental, and finite element analysis is also under research.

ACKNOWLEDGMENT

The authors would like to thank Alex Rodrigues and Sean Journot for their help in the experimental setup as well as Kraton Polymers LLC to provide samples of Kraton G1650, and G1652 for research.

REFERENCES

[1] G. Abdou and N. Atalla, "Applying waterjet technology in surgical procedures," in *Proceedings of the Future Technologies Conference*. Springer, 2018, pp. 616–625.

[2] H. Baer, G. Maddern, and L. Blumgart, "Hepatic surgery facilitated by a new jet dissector," *HPB Surgery*, vol. 4, no. 2, pp. 137–146, 1991.

[3] J. Piek, J. Oertel, and M. Robert Gaab, "Waterjet dissection in neurosurgical procedures: clinical results in 35 patients," *Journal of neurosurgery*, vol. 96, no. 4, pp. 690–696, 2002.

[4] S. Hloch, J. Valicek, and D. Kozak, "Preliminary results of experimental cutting of porcine bones by abrasive waterjet," *Tehnicki Vjesnik-Technical Gazette*, vol. 18, no. 3, pp. 467–470, 2011.

[5] R. Gurunluoglu, "Experiences with waterjet hydrosurgery system in wound debridement," *World Journal of Emergency Surgery*, vol. 2, no. 1, p. 10, 2007.

[6] C. M. Vollmer, E. Dixon, A. Sahajpal, M. S. Cattral, D. R. Grant, S. Gallinger, B. R. Taylor, and P. D. Greig, "Water-jet dissection for parenchymal division during hepatectomy," *HPB*, vol. 8, no. 5, pp. 377–385, 2006.

[7] T. Bahls, F. A. Fröhlich, A. Hellings, B. Deutschmann, and A. O. Albu-Schäffer, "Extending the capability of using a waterjet in surgical interventions by the use of robotics," *IEEE Transactions on Biomedical Engineering*, vol. 64, no. 2, pp. 284–294, 2017.

[8] M. Tenenhaus, D. Bhavsar, and H.-O. Rennekampff, "Treatment of deep partial thickness and indeterminate depth facial burn wounds with water–jet debridement and a biosynthetic dressing," *Injury*, vol. 38, no. 5, pp. S38–S44, 2007.

[9] M. Babaiasl, F. Yang, and J. P. Swensen, "Towards water-jet steerable needles," in *2018 7th IEEE International Conference on Biomedical Robotics and Biomechatronics (Biorob)*. IEEE, 2018, pp. 601–608.

[10] R. A. Mrozek, B. Leighliter, C. S. Gold, I. R. Beringer, H. Y. Jian, M. R. VanLandingham, P. Moy, M. H. Foster, and J. L. Lenhart, "The relationship between mechanical properties and ballistic penetration depth in a viscoelastic gel," *Journal of the mechanical behavior of biomedical materials*, vol. 44, pp. 109–120, 2015.

[11] A. Asadian, R. V. Patel, and M. R. Kermani, "Dynamics of translational friction in needle–tissue interaction during needle insertion," *Annals of biomedical engineering*, vol. 42, no. 1, pp. 73–85, 2014.

[12] S. Misra, K. B. Reed, B. W. Schafer, K. Ramesh, and A. M. Okamura, "Mechanics of flexible needles robotically steered through soft tissue," *The International journal of robotics research*, vol. 29, no. 13, pp. 1640–1660, 2010.

[13] R. J. Roesthuis, N. J. van de Berg, J. J. van den Dobbelsteen, and S. Misra, "Modeling and steering of a novel actuated-tip needle through a soft-tissue simulant using fiber bragg grating sensors," in *Robotics and Automation (ICRA), 2015 IEEE International Conference on*. IEEE, 2015, pp. 2283–2289.

[14] S. Misra, K. B. Reed, A. S. Douglas, K. Ramesh, and A. M. Okamura, "Needle-tissue interaction forces for bevel-tip steerable needles," in *Biomedical Robotics and Biomechatronics, 2008. BioRob 2008. 2nd IEEE RAS & EMBS International Conference on*. IEEE, 2008, pp. 224–231.

[15] P. N. Wells and H.-D. Liang, "Medical ultrasound: imaging of soft tissue strain and elasticity," *Journal of the Royal Society Interface*, vol. 8, no. 64, pp. 1521–1549, 2011.

[16] F. Yang, M. Babaiasl, and J. P. Swensen, "Fracture-directed steerable needles," *Journal of Medical Robotics Research*, p. 1842002, 2010.